Am J Physiol Endocrinol Metab 306: E1033–E1045, 2014.
First published March 4, 2014; doi:10.1152/ajpendo.00422.2013.

Proinflammatory cytokines differentially regulate adipocyte mitochondrial metabolism, oxidative stress, and dynamics

Wendy S. Hahn,[1] Jovan Kuzmicic,[2] Joel S. Burrill,[1] Margaret A. Donoghue,[1,3] Rocio Foncea,[1] Michael D. Jensen,[4] Sergio Lavandero,[2,5] Edgar A. Arriaga,[3] and David A. Bernlohr[1]

[1]*Department of Biochemistry, Molecular Biology, and Biophysics, University of Minnesota, Minneapolis, Minnesota;* [2]*Advanced Center for Chronic Diseases and Centro Estudios Moleculares de la Célula, Facultad Ciencias Quimicas y Farmaceuticas y Facultad Medicina, Universidad de Chile, Santiago, Chile;* [3]*Department of Chemistry, University of Minnesota, Minneapolis, Minnesota;* [4]*Endocrine Research Unit, Mayo Clinic, Rochester, Minnesota; and* [5]*University of Texas Southwestern Medical Center, Dallas, Texas*

Submitted 31 July 2013; accepted in final form 28 February 2014

Hahn WS, Kuzmicic J, Burrill JS, Donoghue MA, Foncea R, Jensen MD, Lavandero S, Arriaga EA, Bernlohr DA. Proinflammatory cytokines differentially regulate adipocyte mitochondrial metabolism, oxidative stress, and dynamics. *Am J Physiol Endocrinol Metab* 306: E1033–E1045, 2014. First published March 4, 2014; doi:10.1152/ajpendo.00422.2013.—Proinflammatory cytokines differentially regulate adipocyte mitochondrial metabolism, oxidative stress, and dynamics. Macrophage infiltration of adipose tissue and the chronic low-grade production of inflammatory cytokines have been mechanistically linked to the development of insulin resistance, the forerunner of type 2 diabetes mellitus. In this study, we evaluated the chronic effects of TNFα, IL-6, and IL-1β on adipocyte mitochondrial metabolism and morphology using the 3T3-L1 model cell system. TNFα treatment of cultured adipocytes led to significant changes in mitochondrial bioenergetics, including increased proton leak, decreased $\Delta\Psi_m$, increased basal respiration, and decreased ATP turnover. In contrast, although IL-6 and IL-1β decreased maximal respiratory capacity, they had no effect on $\Delta\Psi_m$ and varied effects on ATP turnover, proton leak, or basal respiration. Only TNFα treatment of 3T3-L1 cells led to an increase in oxidative stress (as measured by superoxide anion production and protein carbonylation) and C16 ceramide synthesis. Treatment of 3T3-L1 adipocytes with cytokines led to decreased mRNA expression of key transcription factors and control proteins implicated in mitochondrial biogenesis, including PGC-1α and eNOS as well as deceased expression of COX IV and Cyt C. Whereas each cytokine led to effects on expression of mitochondrial markers, TNFα exclusively led to mitochondrial fragmentation and decreased the total level of OPA1 while increasing OPA1 cleavage, without expression of levels of mitofusin 2, DRP-1, or mitofilin being affected. In summary, these results indicate that inflammatory cytokines have unique and specialized effects on adipocyte metabolism, but each leads to decreased mitochondrial function and a reprogramming of fat cell biology.

mitochondria; cytokine; fusion; adipocyte; respiration

THE ADIPOSE ORGAN IS HIGHLY SPECIALIZED in storage and release of energy in times of nutrient excess and deficit, respectively (11, 30). It also plays a vital role in communicating to the brain and other tissues as to the energy status of the entire organism and hence, can influence feeding behavior and energy utilization (9, 21, 52). Low-grade chronic inflammation of adipose tissue has been characterized as a hallmark of obesity and insulin resistance (14, 17, 50). Current models of obesity-linked adipose inflammation include leukocyte infiltration, increased levels of proinflammatory cytokines such as monocyte chemotactic protein-1, tumor necrosis factor-α (TNFα), interleukin-6 (IL-6), and interleukin-1β (IL-1β) and increased oxidative stress (14, 23). The dysfunction of the adipose tissue that occurs in the metabolic syndrome includes increased lipolysis in a fed state (20, 34) and alterations in adipokine secretion (8, 16), promoting the hypothesis that adipose inflammation underlies the metabolic syndrome and forms a platform for systemic dysfunction.

In adipose tissue, macrophage infiltration leads to the production of reactive oxygen species (ROS) and increased oxidative stress in visceral depots (32, 35, 54). Production of ROS (and related reactive nitrogen species) results in oxidative damage to phospholipids, proteins, and DNA. Pathways for ROS formation are numerous and include superoxide ($O_2^{-\cdot}$) production via activation of NADPH oxidase, the 5/12/15 lipoxygenase system, xanthine oxidase, and mitochondrial complexes I and III (10, 17). Hydrogen peroxide production occurs at numerous sites such as peroxisomal fatty acid oxidation, lysyl oxidase, and several dihydrolipoamide dehydrogenase-containing enzyme systems such as pyruvate dehydrogenase, α-ketoglutarate dehydrogenase, and branched-chain keto acid dehydrogenase (1, 47) as well as via mitochondrial and cytoplasmic superoxide dismutase (37). As such, ROS generation occurs in multiple locations and can be regulated by a large number of metabolic, hormonal, and genetic determinants.

Although it is broadly appreciated that proinflammatory cytokines lead to adipocyte insulin resistance and mitochondrial dysfunction, the specific effects of such cytokines on mitochondrial dynamics have not been fully characterized. Mitochondria are highly dynamic and move along microtubules, and they fuse and fragment in response to stress stimuli and energy demands (33, 59). Fission proteins dynamin-related protein 1 (DRP-1), MiD49/50, and fission protein 1 (FIS1) mediate biogenesis of new organelles as well as quality control and mitophagy through mitochondrial fragmentation (59). Conversely, fusion of mitochondria is mediated by mitofusin 1/2 and optic atrophy 1 (OPA1) localized on the outer and inner membranes, respectively. Mitochondrial fusion is thought to be a mechanism for quality control where mitochondria can share DNA, proteins, and metabolic substrates under conditions of stress or nutrient deprivation (51).

The current study was undertaken to characterize the role(s) of inflammatory cytokines on mitochondrial activity, morphol-

Address for reprint requests and other correspondence: D. A. Bernlohr, Dept. of Biochemistry, Molecular Biology, and Biophysics, Univ. of Minnesota, 321 Church St. SE, Suite 6-155, Minneapolis, MN 55455 (e-mail: Bernl001@umn.edu).

ogy, and dynamics with the goal of identifying molecular mechanisms that link inflammation and oxidative stress to cellular function. As opposed to an in vivo approach using high-fat-fed animals where multiple cytokines concurrently affect cellular function, we undertook a more focused approach using specific cytokines and their chronic effect in the 3T3-L1 adipocyte model system. In this report, we define the role(s) of individual cytokines on key parameters affecting adipocyte mitochondrial function/respiration, dynamics, and morphology.

EXPERIMENTAL PROCEDURES

Reagents. Mouse recombinant TNFα, IL-1β, and IL-6 were purchased from R & D Systems (Minneapolis, MN). Oligomycin, carbonylcyanide p-triflouromethoxyphenylhydrazone (FCCP) and Antimycin A were purchased from Sigma (St. Louis, MO). Trizol was purchased from Invitrogen (Grand Island, NY). EZ-link Biotin Hydrazide and IR-800 Streptavidin were purchased from Thermo Scientific (Rockford, IL). Antibodies were purchased from the following companies; manganese superoxide dismutase, mitofillin, and cleaved caspase-3 were from R & D Systems (Minneapolis, MN), mitofusin 2 (MFN2) and OPA1 were from Abcam (Cambridge, MA), DRP-1 was from BD Transduction Laboratories (San Jose, CA), FIS1 antibody was purchased from Alexis/Enzo (Farmingdale, NY), cytochrome *c* oxidase subunit IV (COX IV) antibody was from Cell Signaling Technology (Danvers, MA), perilipin NH_2-terminal antibody was from American Research Products (Belmont, MA), and β-actin was from Sigma (St. Louis, MO). MitoTracker green FM, triphenylphosphonium hydroethidine (TPP-HE; MitoSOX), and tetramethylrhodamine methyl ester (TMRM) were purchased from Molecular Probes (Grand Island, NY).

Cell culture. 3T3-L1 fibroblasts were grown to confluence in DMEM containing 25 mM glucose, 1× glutamax (Invitrogen, Carlsbad, CA), supplemented with penicillin, streptomycin, and 10% calf serum. At 2 days postconfluence (*day 0*), cells were switched to differentiation media containing DMEM with 25 mM glucose and 1× glutamax, 10% fetal bovine serum (FBS), 1 μg/ml insulin, 100 ng/ml dexamethasone, 115 μg/ml isobutylmethylxanthine, and 5 μM troglitazone (Sigma, St. Louis, MO) for 2 days. After 2 days the dexamethasone, isobutylmethylxanthine, and troglitazone were withdrawn. Beginning on *day 4*, the differentiated adipocytes were maintained in high-glucose DMEM with 10% FBS. Differentiation was evaluated by the acquisition of the adipocyte morphology, expression of adipocyte marker proteins such as FABP4, and lipid accumulation.

Cytokine treatment. Each cytokine was reconstituted in 0.1% fatty acid-free BSA (Sigma) to a working concentration of 10 ng/ml. Beginning on *day 6*, 3T3-L1 adipocytes were treated with 1 nM TNFα, IL-6, or IL-1β in DMEM containing 10% FBS for 96, 48, or 24 h. Medium with cytokines was refreshed daily, and assays were performed 8–11 days postdifferentiation.

Cell respiratory control. Cellular respiration and proton efflux were analyzed using the XF24 Analyzer and system software (Seahorse Bioscience, Billerica, MA). 3T3-L1 fibroblasts were grown and differentiated as described above in XF24 V7 culture dishes coated with 0.2% gelatin (Sigma). Adipocytes were treated with or without (control) 1 nM of each cytokine for 24–96 h in complete medium prior to the assay (6). On *day 10* postdifferentiation, cells were washed with and switched to serum-free modified, no-bicarbonate, low-phosphate DMEM (D5030) supplemented with 1× glutamax (Invitrogen), 1 mM sodium pyruvate, 25 mM glucose, and 0–1 nM cytokine and allowed to equilibrate for 1 h in a non-CO_2 37°C incubator. After cartridge calibration, cells were placed in the XF24 analyzer, where cellular oxygen consumption and extracellular acidification rate were measured four times under basal conditions and then three times after the addition of 2.5 μM oligomycin through *port A*, three times after 2.5 μM FCCP addition through *port B*, and twice after 4 μM antimycin A addition through *port C*. Measurement protocol for each condition was as follows: mix for 2 min, wait for 2 min, and measure for 2 min. Time points ($n = 4$) for each cytokine were assayed simultaneously. Oxygen consumption rate (pmol/ min) and extracellular acidification rate (ECAR; mpH/min) data obtained from the Seahorse XF24 Software were normalized to the untreated control (100%) for graphing purposes.

2-Deoxyglucose uptake assay. Cellular uptake of 2-deoxyglucose was assessed in 3T3-L1 adipocytes treated for 24 h with 1 nM of indicated cytokine in complete medium beginning on *day 9* of differentiation. On *day 10*, cells were washed in PBS and incubated for 2 h in serum-free HEPES buffer (3.8 mM HEPES, 2 mM $NaHCO_3$, 120 mM NaCl, 4.7 mM KCl, 1.2 mM pyruvate, 3.2 mM $CaCl_2$, and 0.5% fatty acid free BSA, pH 7.4) supplemented with 1 nM cytokine. Uptake assay was initiated by adding 2-deoxyglucose to a final concentration of 100 μM at 0.5 μCi 2-[^{3}H]deoxyglucose /ml. Cells were incubated for 5 min at 37°C and 5% CO_2. Uptake was terminated by washing three times with ice-cold PBS. Cells were lysed in 1% Triton X-100, and lysate was subjected to scintillation counting. Intracellular 2-[^{3}H]deoxyglucose was determined by linear regression of a standard curve of known concentrations.

Nonesterified fatty acid efflux. Fatty acid efflux from adipocytes treated with cytokines was assessed in nutrient conditions similar to those used in respiration studies. Serum-free modified DMEM (D5030; Sigma) supplemented with 1 mM glutamax, 1 mM sodium pyruvate, 25 mM glucose, an d 0–1 nM cytokine with 2% fatty acid-free BSA was placed on washed cells after a 24-h cytokine treatment. Assay medium was collected after 1 h, and replicate measurements of free fatty acids were determined spectrophotometrically using the NEFA-C kit (Wako Chemicals, Richmond, VA) according to the manufacturer's protocol.

Cellular NAD^+/NADH levels. 3T3-L1 adipocytes were grown in six-well plates and treated with cytokine, as described earlier. Cells were washed twice in ice-cold PBS, pelleted by centrifugation, all liquid was removed, and the resultant pellet was frozen on liquid nitrogen. Cell pellets were thawed and replicate samples used to determine NAD^+ or NADH levels using the EnzyChrom NAD^+/NADH Assay Kit (BioAssay Systems, Hayward, CA) according to the manufacturer's instructions. Levels of nicotinamide adenine dinucleotide were normalized to protein content determined by bicinchoninic acid assay (Sigma).

Mitochondrial superoxide analysis. Production of superoxide was measured in differentiated 3T3-L1 cells based on previously described procedures (15, 56). The medium containing cytokines was removed and replaced with fresh me-

dium containing 10% FBS, 10 μM TPP-HE, and 100 nM rhodamine 123 (R123) for 60 min. at 37°C. Cells were then washed with PBS, suspended in 15 μg/ml digitonin, and incubated on ice for 20 min to remove the residual cytoplasmic probe. The resultant cell pellet was lysed and treated with 2 mg/ml proteinase K for 45 min, followed by 400 U/ml DNase I for 30 min at 37°C to digest the DNA present in the sample. Samples were diluted 1:5 in run buffer (10 mM borate-1 mM CTAB, pH 9.3) and analyzed by micellar electrokinetic chromatography with laser-induced fluorescence detection (MEKC-LIF) to measure OH-TPP-E+ and R123.

Mitochondrial membrane potential. 3T3-L1 adipocytes grown in 12-well plates were treated for 24 h with or without 1 nM cytokine ($n = 4–7$). Live cells were stained by the addition of 200 nM TMRM (Invitrogen) and incubated in complete medium with or without cytokine for 30 min. at 37°C, 5% CO_2. A depolarization control was included by adding 500 nM FCCP for 5 min prior to TMRM staining. Cells were then washed three times in PBS and removed from culture dish by incubation with 1× phenol red-free trypsin in KRH for 5 min at room temperature, followed by inactivation with 10% vol/vol FBS. Cells were then transferred to a FACS tube while passing through a 70-μm cell strainer. Cell samples were run on a Becton Dickinson cell analyzer with FACSDiva software (BD Biosciences, San Jose, CA) using the parameters PE 220V, FSC 500V, and SSC 230V. Counts were gated, and mean PE fluorescence from 10,000 cells was used to calculate average TMRM fluorescence sample. Data are reported as means ± SE, and statistical significance was determined using the Student's *t*-test.

Protein carbonylation. Protein carbonyls were detected as described previously (15, 19). Briefly, cells were washed and scraped into buffer containing 100 mM sodium acetate, 10 mM sodium chloride, 0.1 mM EDTA, pH 5.5, complete mini protease inhibitors (Roche), pepstatin, and phosphatase inhibitors (Sigma). Cells were lysed by sonication, and lipid was separated by low-speed centrifugation. After the lipid cake was removed, lysates were supplemented with 1% SDS, mixed, and centrifuged at 100,000 *g* for 1 h. Protein concentration was determined by the bicinchoninic acid method, and 25 μg of total protein was incubated with 0.5 mM biotin hydrazide (Pierce, Rockford, IL) for 3 h at room temperature. The reaction mixture was subjected to SDS-PAGE using a 5–20% acrylamide gel, and proteins were transferred to PVDF-immobilon FL membrane (Millipore, Billerica, MA). The membrane was blocked in Licor blocking buffer, incubated with IR-800 Streptavidin (Pierce), diluted 1:15,000 in PBS with 0.1% Tween-20 for 1 h, and washed thoroughly, and carbonylated proteins were visualized using LI-COR Odyssey infrared imager (LI-COR, Lincoln, NE) and quantified with the software provided by the manufacturer.

Sphingolipid analysis. The cellular content of sphingolipids was measured using a UPLC/MS/MS approach, as described previously (4, 5). Briefly, the cells were washed three times in ice-cold PBS and centrifuged at 700 *g*, and the resultant pellet was flash-frozen in liquid nitrogen. Cell pellets were thawed and homogenized in 100 μl of PBS, pH 7.4. Homogenates were supplemented with internal standard solution consisting of ^{17}C-sphingosine, ^{17}C-S1P, and ^{17}C16-Cer (Avanti Polar Lipids) as well as an extraction mixture [isopropanol-water-ethyl acetate, 30:10:60 (vol/vol/vol)]. The mixture was vortexed, sonicated, and centrifuged for 10 min at 12,000 rpm at 4°C. The supernatant was transferred to new tube and evaporated under nitrogen. The dried sample was reconstituted in 100 μl of LC Solvent A (1 mM ammonium formate, 0.1% formic acid in methanol) for ultra performance liquid chromatography/mass spectrometry/mass spectrometry (UPLC/MS/MS) analysis on a Waters Acquity UPLC system (Milford, MA) coupled with a Thermo TSQ Quantum Ultra mass spectrometer (Waltham, MA).

Mitochondrial isolation. 3T3-L1 adipocytes were scraped on ice-cold isolation buffer (20 mM Tris·HCl, 220 mM mannitol, 70 mM sucrose, 1 mM EDTA, and 0.1 mM EGTA, pH 7.4) containing protease inhibitors (Invitrogen). Cells were lysed with 20 strokes of a glass/teflon homogenizer, and the resulting homogenate was centrifuged at 700 *g* for 10 min at 4°C. The supernatant was transferred to a new tube and centrifuged at 10,000 *g* for 20 min, and the cytosolic fraction was collected. The pellet was washed once with isolation buffer, centrifuged again at 10,000 *g* for 10 min, and resuspended in fresh isolation buffer supplemented with 1% Triton X-100 and 0.1% SDS. This fraction represents a mitochondrial enriched extract.

mRNA expression. Expression of mRNAs was measured by quantitative RT-PCR. Total RNA was isolated was isolated using TRIzol reagent according to manufacturer's protocol. RNA was treated with DNase I and cDNA synthesized using iScript cDNA synthesis kit (Bio-Rad, Hercules, CA). Amplification was monitored with iQ SYBRgreen Supermix and the MyiQ detection system (Bio-Rad, Hercules, CA). Table 1 contains the primer sequences used to amplify and detect target transcripts. Relative expression was calculated using the $2^{(-\Delta\Delta C_T)}$ method. Data are reported as means ± SE, and statistical significance was determined using the Student *t*-test.

Western blot. Cells treated with cytokine as stated previously were washed three times in ice-cold PBS and lysed in buffer containing 50 mM NaCl, 1 mM EDTA, 1 mM EGTA, 50 mM NaF, 1 mM NaP_2O_7, 1% Triton X-100, 0.1% SDS, 1× Complete Mini Protease Inhibitor (Roche), 1 × phophatase inhibitor I, and 1 × phophatase inhibitor II (Sigma).

Equal amounts of protein were separated by SDS-PAGE, transferred to PDVF Immobilon-FL (Millipore) membrane, and blocked with 50% Licor blocking buffer in phosphate-buffered saline (PBS). Blocked membranes were incubated with indicated primary antibodies overnight and reblotted with

Table 1. *Primers used for quantitative real-time PCR*

mRNA	Accession No.	Forward and Reverse Primers
Tfam	NM_009360	Forward: CACTGGGAAACCACAGCATACAG
		Reverse: GGACATCTGAGGAAAAGCCTTGC
PGC-1α*	NM_008904	Forward: CACGAAAGGCTCAAGAGGGATG
		Reverse: CACCAAAAACTTCAAAGCGGTCTC
eNOS	NM_008713	Forward: TGTCTGCGGCGATGTCACTATG
		Reverse: CGAAAATGTCCTCGTGGTAGCG
NRF1	NM_010938	Forward: TGGTCCAGAGAGTGCTTGTGAAG
		Reverse: GGAGGCTGAGGAACGATTTCTTG
TFIIE	NM_026584	Forward: CAAGGCTTTAGGGGACCAGATAC
		Reverse: CATCCATTGACTCCACAGTGACAC

Tfam, transcription factor A mitochondria; PGC-1α, peroxisome proliferator-activated receptor-γ coactivator-1α; eNOS, endothelial nitric oxide synthase; TFIIE, transcription factor IIE. The forward and reverse primers for the *mus musculus* mRNAs quantified by quantitative real-time PCR are indicated. *All PGC-1α splice variants are recognized by this primer set.

anti-rabbit or anti-mouse secondary antibodies conjugated to LI-COR IRDye for 1 h at room temperature. The bands were detected using a LI-COR Odyssey infrared imager (LI-COR Biotechnologies) and quantified with the software provided by the manufacturer. Protein content was normalized to an internal loading control such as β-actin or mitofilin.

Mitochondrial imaging. Cells were grown and differentiated in a six-well plate containing 25-mm round glass coverslips. For mitochondrial staining, cells were incubated in 300 nM MitoTracker green in KRH buffer at 37°C for 30 min. The cells were washed and maintained in KRH supplemented with 1% BSA and observed under an Olympus Deltavision Personal DV microscope using a ×100/1.4 oil objective at 25°C. The software SoftWoRx version 4.1.2 was used to acquire and deconvolve the images. Thirty to 35 Z-stacks of 0.30-μm thickness per cell were obtained. The Image J plug-in Volume J was used to reconstitute the Z-stacked images. Cells showing a fragmented pattern of mitochondria were counted manually, and changes in mitochondrial number and mean volume were quantified using the Image J-3D Object counter plug-in for Image J. Each experiment was performed six times, and 16–25 cells/condition were quantified. An increase in fragmentation pattern and in mitochondrial number, together with a decrease in mean mitochondrial volume, was considered fission criteria (41).

Statistical analysis. Data are means ± SE of the indicated sample size (n). Student's t-test was performed for comparisons between two groups. Multiple groups were analyzed using one-way ANOVA, followed by a protected Tukey test. Statistical significance was defined as $P < 0.05$.

RESULTS

Proinflammatory cytokines have distinct effects on adipocyte respiration profiles. Chronic treatment of 3T3-L1 adipocytes with each of the proinflammatory cytokines TNFα, IL-1β, and IL-6 led to distinct changes in mitochondrial respiration. Oxygen consumption in intact 3T3-L1 adipocytes was measured in a basal state and after cells were challenged with oligomycin to inhibit the ATP synthase FCCP to depolarize the inner mitochondrial membrane and antimycin A to inhibit complex III and thus oxygen utilization by the electron transport chain. The concentration dependence of TNFα on mitochondrial respiration was evaluated (10 pM to 1 nM), and effects on basal respiration were detected only on the highest concentration (results not shown), and consequently, 1 nM cytokine was adopted for all of the studies reported herein. Figure 1 profiles the respiration of cells that were treated for 24, 48, or 96 h with 1 nM of indicated cytokine compared with untreated control.

TNFα treatment led to an increase in basal respiration at 24 h that then declined at 48 and 96 h. IL-1β did not change the basal respiration at 24- or 48-h treatment, but it did decrease respiration significantly at 96 h. IL-6 treatment was accompanied by an increase in basal respiration only at the 96-h time point (Fig. 1*A*). Respiration measured after treatment with oligomycin reflects electron flow allowed by proton leak across

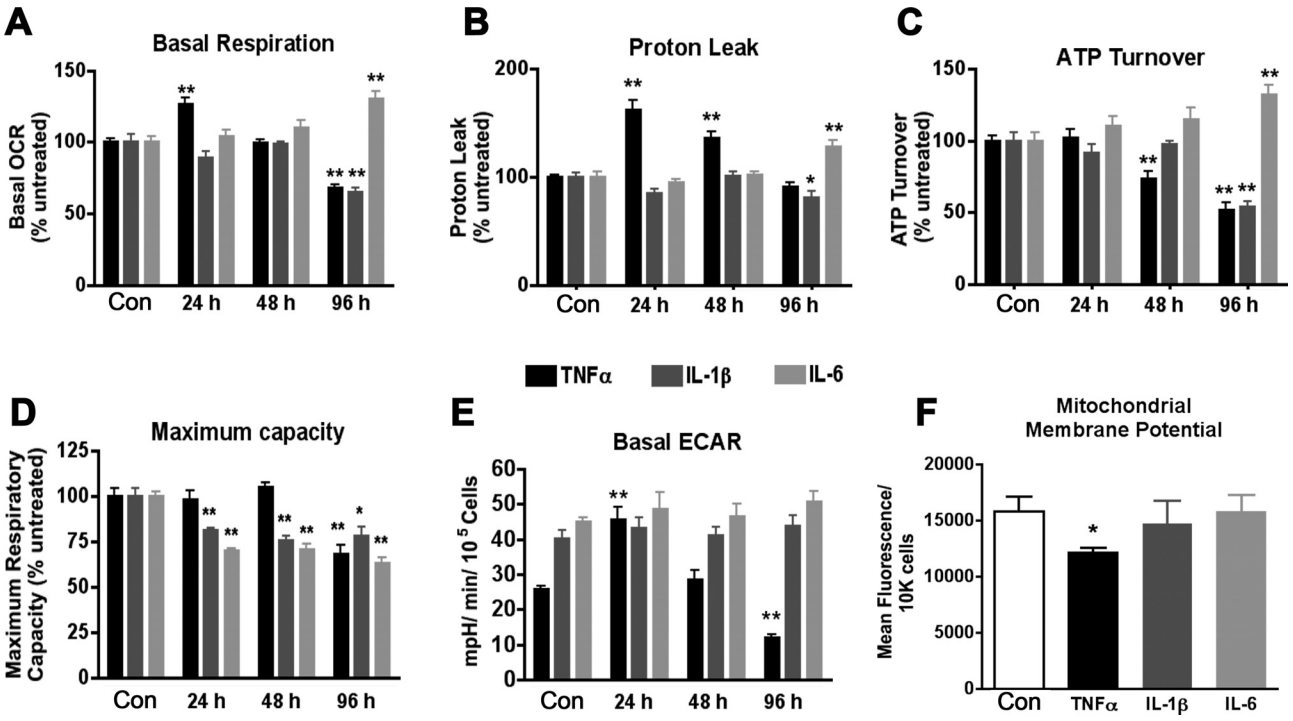

Fig. 1. Respiration profiling in chronic cytokine treatment of 3T3-L1 adipocytes. 3T3-L1 adipocytes were treated with 1 nM of the indicated cytokine in complete medium for 24–96 h beginning on *day 6* of differentiation, and parameters linked to respiration and other biological processes were measured using the Seahorse XF24 Analyzer. *A–D*: values were used to calculate total oxygen consumption due to basal respiration (*A*), inner mitochondrial membrane proton leak (*B*), cellular ATP demand (*C*), and maximum respiratory capacity (*D*). *E*: extracellular acidification rate (ECAR) was compared in cytokine treatments of varying duration under basal respiration conditions. *F*: mitochondrial membrane potential ($\Delta\Psi_m$) was determined in 3T3-L1 adipocytes treated for 24 h with 1 nM cytokine (n = 3) by tetramethylrhodamine methyl ester (TMRM) staining and flow cytometry of 10,000 cells. All data are represented as means ± SE. $^{**}P < 0.005$ and $^{*}P < 0.05$, statistical significance determined by Student's t-test compared with untreated 0-h control; n = 5 unless noted. OCR, oxygen consumption rate.

the inner mitochondrial membrane; thus we calculated the proton leak and ATP turnover. TNFα increased the proton leak significantly at 24 and 48 h, IL-1β caused a modest decrease in the proton leak at 96 h, and IL-6 elevated the proton leak only at the latest 96-h time point (Fig. 1*B*). Respiration coupled to ATP synthesis (ATP turnover) was unchanged by any of the cytokines tested at 24 h. However, TNFα lowered ATP turnover at 48 and 96 h, a decrease that was also observed after 96 h of IL-1β, and an increase was measured after 96 h of IL-6 treatment (Fig. 1*C*). The addition of the proton ionophore FCCP collapses the mitochondrial membrane potential ($\Delta\Psi_m$) and allows for the measurement of maximal oxygen consumption. Figure 1*D* shows that the respiratory capacity remains intact in TNFα treatment at 24 and 48 h but declines after 96 h. IL-1β and IL-6 conversely decrease the maximum capacity at all time points measured.

The ECAR is an indicator of lactate efflux and indirectly assesses reliance of the cells on anaerobic glycolysis. Although the interleukins produced no measurable change in this parameter, TNFα increased ECAR by 1.7-fold at 24 h and then decreased the level by half at 96 h (Fig. 1*E*). Since basal lipolysis from 3T3-L1 adipocytes can be enhanced by proinflammatory cytokines, we hypothesized that the increased ECAR could be due in part to efflux of free fatty acids. Therefore, we measured the nonesterified free fatty acids (NEFAs) after 24 h of cytokine treatment. Figure 2*A* demonstrates that whereas TNFα increased NEFAs in the medium as expected, IL-1β had a similar effect without the concomitant increase in ECAR (Fig. 1*E*). Both TNFα and IL-1β treatment led to a decline in perilipin protein level at 24 h (Fig. 2*B*). Conversely, 1 nM IL-6 exhibited no effect on basal fatty acid efflux (Fig. 2*A*). These data support the conclusion that the observed changes in ECAR are derived from lactate efflux rather that fatty acid efflux and that a loss of perilipin expression may contribute to the increased fatty acid efflux in the absence of lipolytic stimuli. Treatment of adipocytes with TNFα or IL-1β for 24 h also led to a 3.5- or 2-fold increase, respectively, in basal glucose transport, as measured by 2-deoxyglucose uptake (Fig. 2*D*). Interestingly the IL-1β treatment increased glucose uptake and fatty acid efflux without a change in ECAR. The observed metabolic changes were also accompanied by a shift in the redox status. Lower NAD^+/NADH ratios were seen in TNFα and IL-1β treatment at all time points and at 96 h after treatment with IL-6 (Fig. 2*C*).

To parallel the changes in cytokine-induced respiration to changes in the inner $\Delta\Psi_m$, we utilized TMRM staining coupled with flow cytometry analysis. Figure 1*F* reveals that 24-h treatment of 3T3-L1 adipocytes with TNFα decreased TMRM staining intensity by 23%, whereas treatment with IL-1β or IL-6 had no detectable influence on the $\Delta\Psi_m$. These results are consistent with the proton leak detailed in Fig. 1*B*.

Mitochondrial oxidative stress and protein carbonylation are increased by TNFα but not by IL-1β or IL-6. A previous report states that obesity-linked inflammation increases oxidative stress in adipose tissue (17). To assess the effect of specific cytokines on ROS synthesis, superoxide production was evaluated by accumulation of oxidized TPP-HE ($\Delta\Psi_m$ sensitive) normalized to R123 ($\Delta\Psi_m$ sensitive as well) in the mitochondria. Whereas TNFα treatment led to a two-, three-, and 3.5-fold increase in superoxide levels in the mitochondria at 24, 48, and 96 h, respectively, no significant changes were detected in IL-1β- or IL-6-treated cells (Fig. 3*A*).

We hypothesized that the increased superoxide would lead to increased protein carbonylation similar to that observed in adipose from diet-induced obese mice (24). Using IR800-conjugated streptavidin to detect biotin hydrazide conjugated to protein carbonyls, IL-1β or IL-6 shows negligible effects on protein carbonylation compared with control cells (Fig. 3*B*). In contrast, TNFα treatment increased the carbonylation of proteins at 24 h, whereas at longer duration of treatment protein

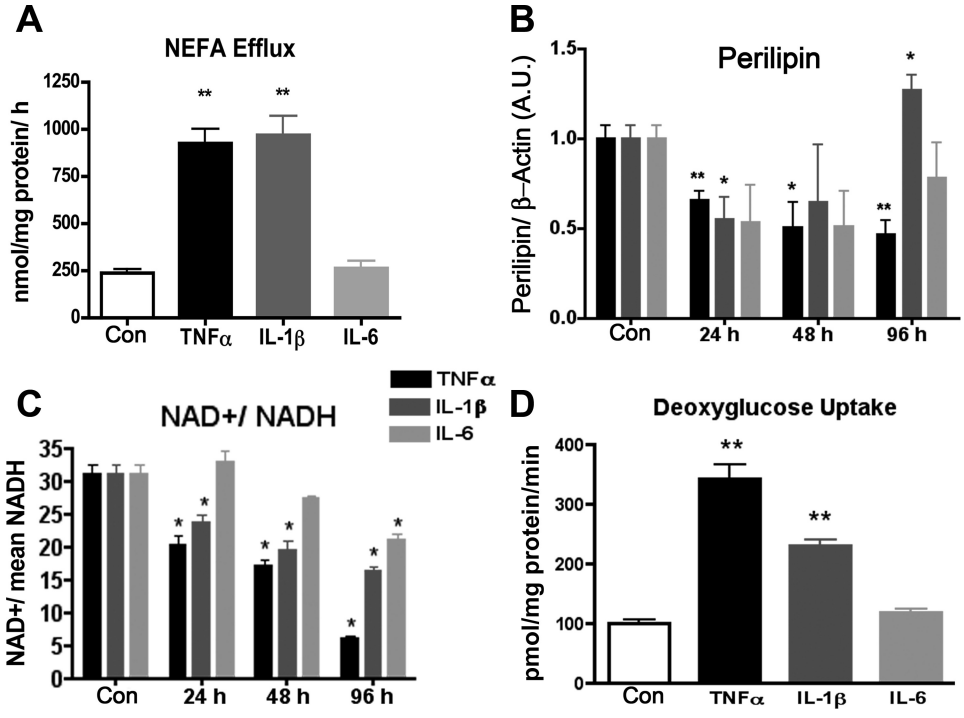

Fig. 2. Lipid and glucose metabolism following cytokine treatment of 3T3-L1 adipocytes. Nonesterified fatty acid (NEFA) efflux (*A*), perilipin abundance (*B*), NAD^+/NADH (*C*), and 2-deoxyglucose uptake (*D*) were measured following 24-h treatment of adipocytes with 1 nM cytokine. In *B*, Western blot quantitation of perilipin protein signal was normalized to β-actin protein signal ($n = 6$). $^*P < 0.05$ and $^{**}P < 0.01$ compared with control.

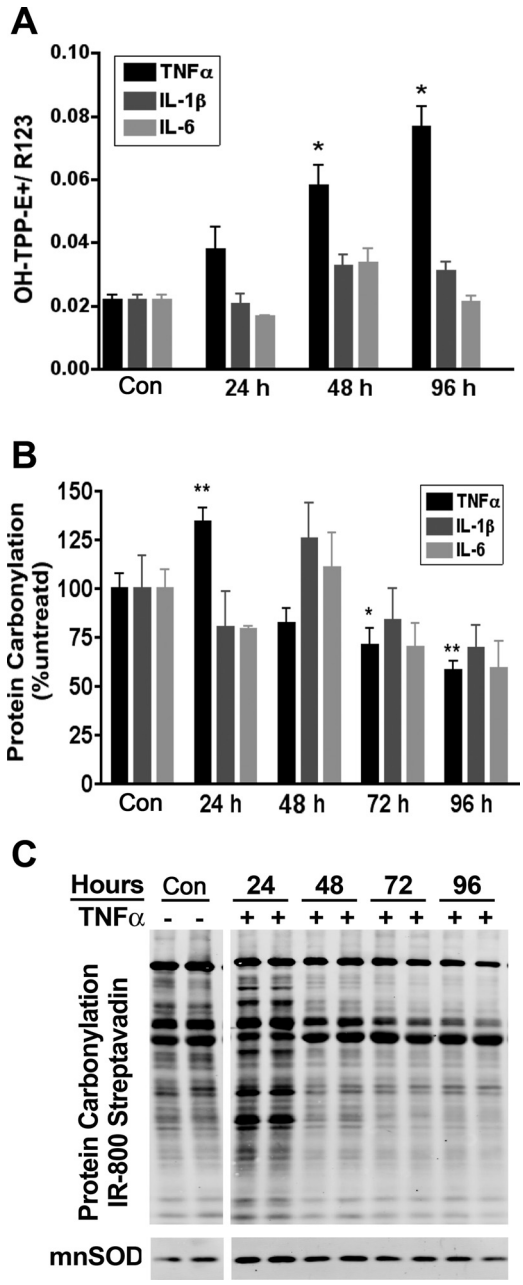

Fig. 3. Reactive oxygen species and protein carbonylation following cytokine treatment of 3T3-L1 adipocytes. *A* and *B*: on *day 6*, 3T3-L1 adipocytes were treated with the indicated cytokine for 24 h, and mitochondrial superoxide formation (*A*) and protein carbonylation (*B*) were evaluated; $n = 3$. *C*: protein carbonylation blot of TNFα treatment for 24–96 h was probed simultaneously with anti-manganese superoxide dismutase (MnSOD). The break in *C* represents a translocation of lanes from the same image and exposure purely for illustration purposes only and does not alter the image information. TPP, triphenylphosphonium hydroethidine. $^{*}P < 0.05$; $^{**}P < 0.01$.

carbonylation was surprisingly decreased (Fig. 3, *B* and *C*). Further investigation revealed that the expression of the mitochondrial superoxide dismutase SOD2 is increased by TNFα treatment at 24 h (Fig. 3*C*). This antioxidant response may in part explain the observation of a decrease in protein carbonyls found at later time points (Fig. 3*C*) despite an increase in superoxide (Fig. 3*A*).

Sphingolipid profiles are selectively altered with cytokine treatment. Compelling evidence suggests a central role for ceramides in the pathology of the metabolic syndrome (28, 58). Moreover, adipocytes robustly produce ceramides in response to high levels of palmitate or in response to proinflammatory stress (4). To address the effects of specific cytokines on sphingolipid synthesis, lipidomic analysis was carried out on 3T3-L1 cells treated with various cytokines. Whereas the total cellular ceramide levels trended toward an increase with TNFα treatment, individual ceramide species showing significant increases included C16 and C18:1 (Fig. 4, *A* and *C*). C24 ceramide levels were not altered by TNFα or IL-1β but decreased in response to IL-6 treatment (Fig. 4*B*). The level of sphingosine 1-phosphate (S1P), a mediator of inflammation and leukocyte trafficking (13), is transiently increased in adipocytes treated with IL-1β but unchanged with IL-6 (Fig. 4*D*). Sphinganine, the de novo synthetic precursor to ceramide, was increased by TNFα and IL-1β treatment but not altered by IL-6 (Fig. 4*F*).

Mitochondrial content and biogenesis markers are altered with cytokine treatment. Previous work by Curtis et al. (15) has shown that TNFα treatment of 3T3-L1 adipocytes led to decreased mRNA expression for glutathione *S*-transferase, a key antioxidant responsible for metabolism of much of the reactive aldehydes produced by cells. To evaluate the effect of cytokines on expression of genes linked to the mitochondrial biogenesis program, quantitative RT-PCR (Table 1) was performed on mRNA isolated from 3T3-L1 adipocytes treated with proinflammatory cytokines for 24 h. Interestingly, none of the cytokines (TNFα, IL-6, or IL-1β) tested significantly al-

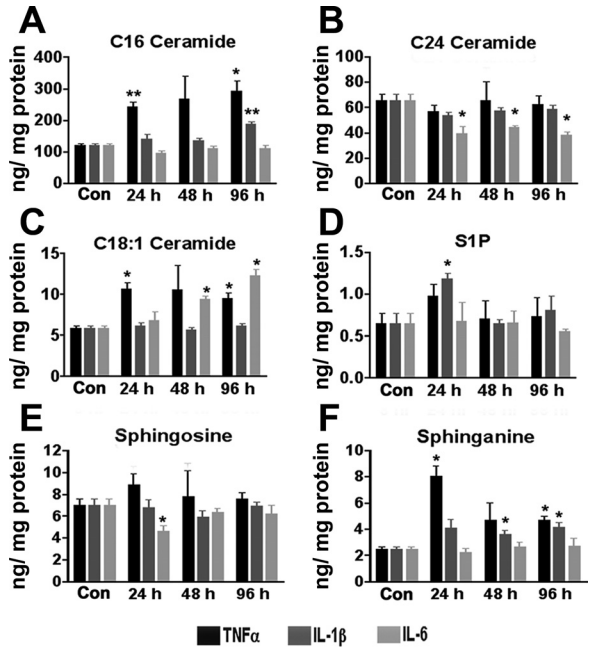

Fig. 4. Sphingolipid profiles following cytokine treatment. 3T3-L1 adipocytes were treated with 1 nM of the indicated cytokine for 0–96 h. At the indicated times, cellular extracts were subject to ultra performance liquid chromatography/mass spectrometry/mass spectrometry and the levels of sphigolipids determined. *A–F*: C16 ceramide (*A*), C24 ceramide (*B*), C18:1 ceramide (*C*), sphingosine-1 phosphate (S1P; *D*), sphingosine (*E*), and sphinganine (*F*). Each bar represents the mean ± SE; $n = 3$. $^{*}P < 0.05$ by Student's *t*-test compared with 0-h control. $^{**}P < 0.01$.

tered the expression level of the transcription factor A mitochondria (Tfam). Expression of nuclear respiration factor 1 was selectively decreased by TNFα (Fig. 5*A*), and all three proinflammatory cytokines significantly reduced the expression of master mitochondiral biogenesis regulators, perixosome proliferator-activated receptor-γ coactivator-1α (PGC-1α), and endothelial nitric oxide synthase (eNOS) (Fig. 5*A*). Consistent with altered mitochondrial biogenesis, TNFα treatment led to a significant decrease in protein levels of nuclear-encoded COX IV and cytochrome *c* (Cyt *c*). However, the abundance of the inner membrane-associated protein mitofilin remained unchanged with cytokine treatment (Fig. 5, *B* and *C*). Interleukin 1β also decreased COX IV protein levels, but this effect was only present at 48 h of treatment and returned to basal levels by 96 h. IL-6 treatment caused a similar transient decrease in total Cyt *c* levels at 48 h (Fig. 5, *B* and *C*).

Mitochondrial content and network morphology is altered by TNFα. To determine the effect of inflammatory cytokines on mitochondrial dynamics, we evaluated mitochondrial content and network morphology using fluorescence microscopy. As shown in Fig. 6, treatment of 3T3-L1 adipocytes with TNFα induced significant mitochondrial fragmentation, as revealed by an increase in the number of mitochondria per cell and a decrease in mean volume per mitochondrion compared with control cells. The number of cells exhibiting fragmented mitochondrial morphology was also increased by TNFα treatment (Fig. 6*D*). In contrast, IL-6 or IL-1β treatment had no significant effect on mitochondrial morphology or fragmentation. Since apoptosis is accompanied by fission of mitochondria (59), we next investigated levels of apoptotic effector cleaved caspase-3 and found that TNFα alone induced the apoptotic program, as revealed by caspase-3 cleavage (Fig. 6*E*). The activation of caspase-3 and induction of apoptosis has been reported in adipose from both high-fat-fed mice and obese humans (2).

Since mitochondrial morphology is acutely controlled through the expression, processing, and localization of several

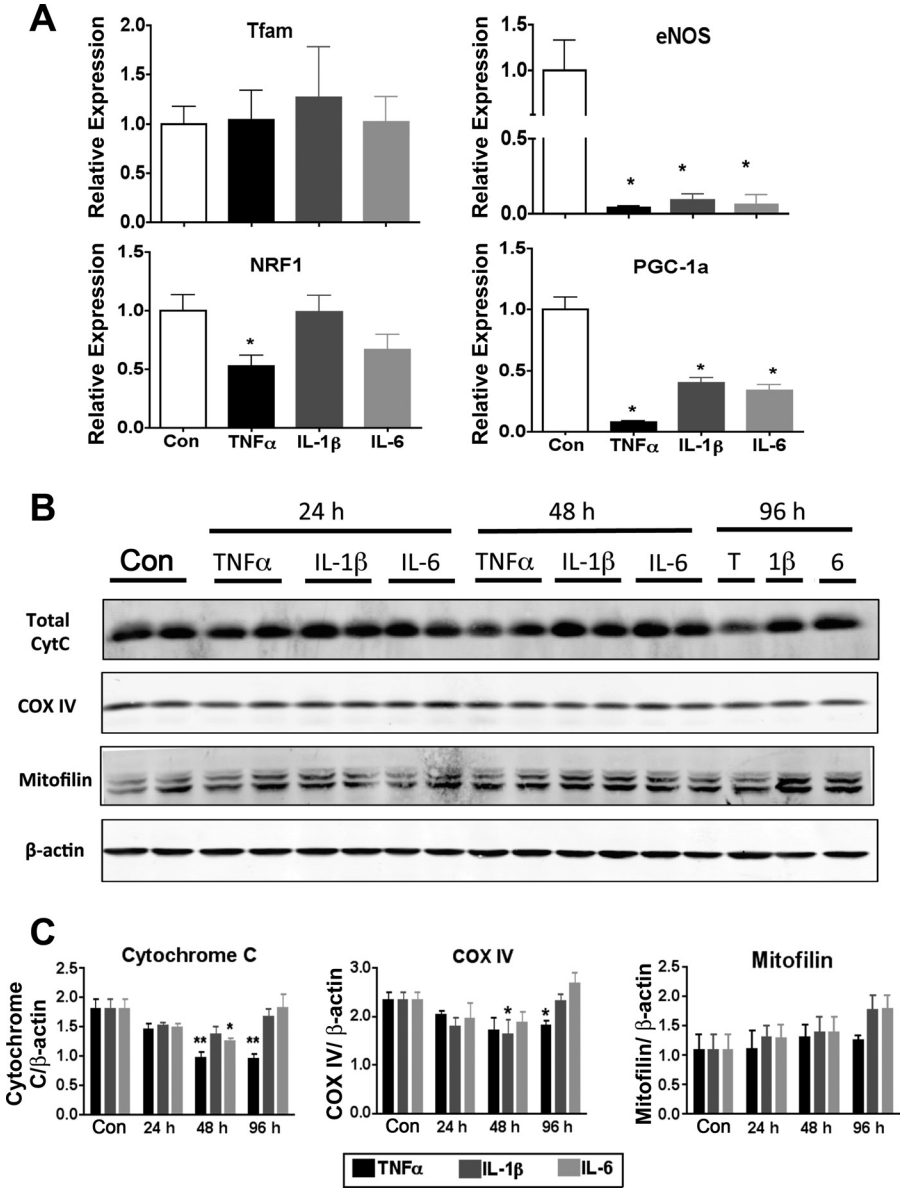

Fig. 5. Expression of factors linked to mitochondrial biogenesis and function in response to cytokine treatment. 3T3-L1 adipocytes were treated with 1 nM of the indicated cytokine for 24 h, and the mRNA (*A*) and protein (*B* and *C*) expression of factors linked to mitochondrial biogenesis and function were evaluated. *B*: Western blot analysis of adipocytes. *C*: quantitation of each protein was normalized to β-actin and graphed relative to control ($n = 6$). QPCR results were normalized to reference mRNA transcription factor IIE. In *A*, the graph of endothelial nitric oxide synthase (eNOS) expression has a broken *y*-axis so that the TNFα treatment group is visible. Tfam, transcription factor A mitochondria; NRF1, nuclear respiratory factor 1; PGC-1α, PPARγ coactivator-1α; Con, control; T, TNFα; 1β, IL-1β; 6, IL-6; Cyt *c*, cytochrome *c*; COX IV, cytochrome *c* oxidase subunit IV. $*P < 0.05$.

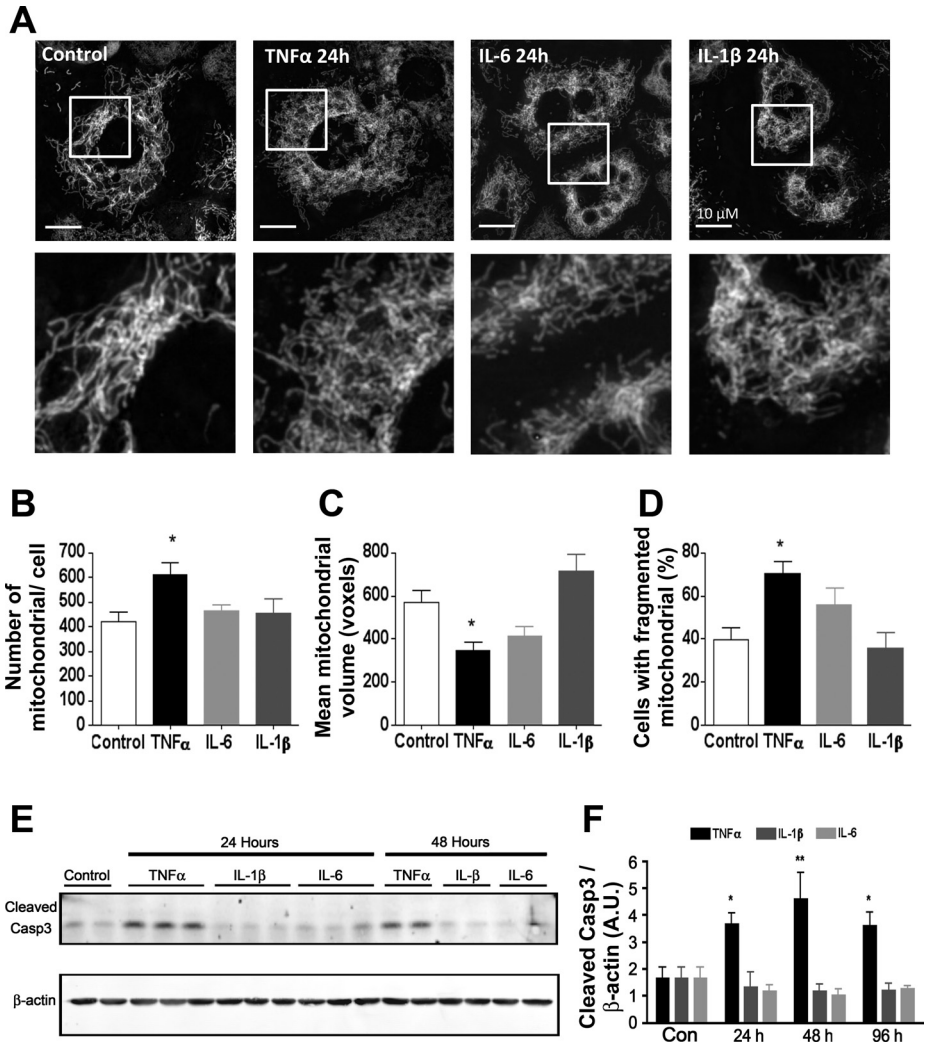

Fig. 6. Mitochondrial morphology in cytokine-treated 3T3-L1 adipocytes. *A*: live cell images of MitoTracker green-stained 3T3-L1 adipocytes after 24-h treatment with 1 nM cytokine. *B* and *C*: images of >15 cells were analyzed using Image J 3D software to determine average mitochondrial no. (*B*) and average volume per mitochondrion (*C*); $n = 5–13$. *D*: each of the cells sampled was scored for mitochondrial fragmentation, and the %cells exhibiting fission was calculated; $n = 6–16$ for each treatment. *E*: Western blot of whole cell extract detecting cleaved caspase-3 and β-actin. *F*: densitometric analysis of cleaved caspase-3 Western blots; $n = 4–6$. $^{*}P < 0.05$ compared with control. $^{**}P < 0.01$.

key regulatory proteins (33, 43), we analyzed the effects of cytokine treatment on the expression of fusion proteins OPA1 and MFN2 and fission protein FIS1 as well as DRP-1 levels and localization. Treatment of 3T3-L1 with TNFα induced a significant reduction in the level of OPA1. Closer inspection reveals a greater disappearance of the short (S) than the long (L) isoform of OPA1 compared with controls (Fig. 7, *A* and *B*). No significant changes in OPA1 expression or processing were observed with IL-6 or IL-1β treatment. In contrast, expression of the outer membrane fusion protein MFN2 was not altered by any of the cytokine treatments analyzed (Fig. 7, *C* and *D*). We next investigated the expression of FIS1, a mitochondrial protein thought to direct the localization of cytosolic DRP-1 to the mitochondria. Once localized at the mitochondria, DRP-1 can form a ring around the organelle, facilitating constriction and fission (59). Total cellular expression of FIS1 and DRP-1 was not changed with cytokine treatment (data not shown). Likewise, the mitochondrial localization of DRP-1 did not significantly change with any of the cytokines analyzed (Fig. 7, *C* and *D*). These results suggest the decrease in expression and/or an increase in processing of OPA1 as the primary effector of increased mitochondrial fragmentation seen in TNFα-treated adipocytes (Fig. 6).

TNFα-induced respiration precedes caspase-3 activation and mitochondrial fragmentation. To determine whether the altered mitochondrial function and morphology measured after TNFα treatment was linked to apoptosis, we evaluated oxygen consumption and morphological analyses relative to caspase-3 cleavage. As shown in Fig. 8*A*, caspase-3 cleavage is evident as early as 2 h after TNFα treatment. By comparison, basal respiration is significantly increased 50% after 1 h of TNFα treatment (Fig. 8*B*). However, mitochondrial morphology was not affected by TNFα until 6 h posttreatment (Fig. 8, *C* and *D*). Taken together, these analyses reveal that TNFα first alters respiration and then activates the apoptotic pathway and eventually causes mitochondrial fragmentation (Figs. 6 and 8).

DISCUSSION

Visceral obesity is accompanied by infiltration of adipose depots with proinflammatory macrophages and T cells, leading to the working model that immune cell factors drive the progression from insulin sensitivity to insulin resistance (14, 23, 35, 45). In a variety of obese animal models both nutritional and genetic, mitochondrial dysfunction has been correlated with inflammation and increased oxidative stress (17).

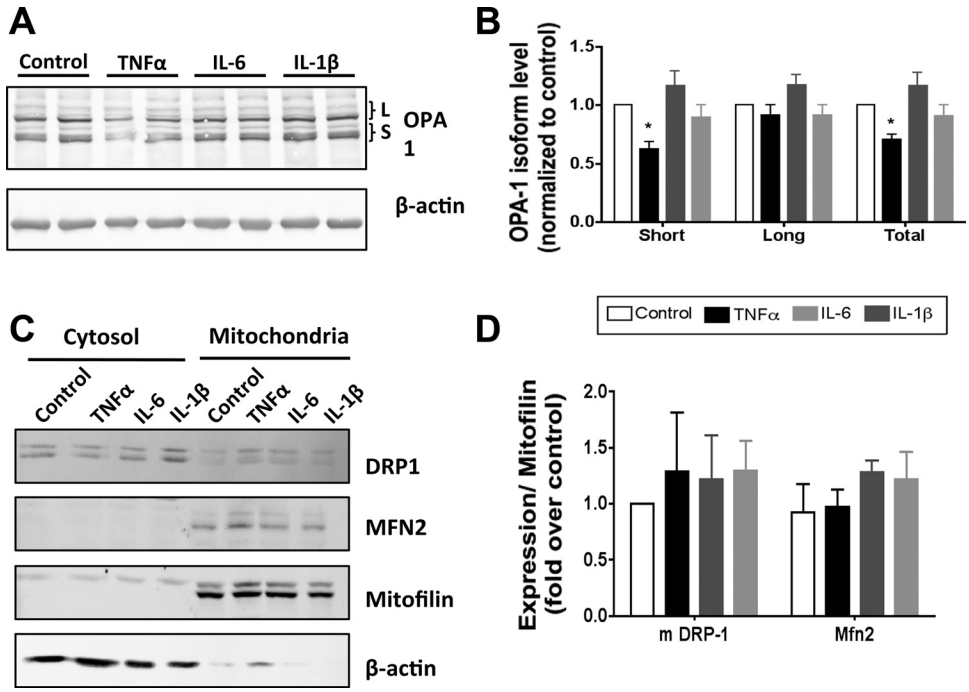

Fig. 7. Expression of proteins linked to mitochondrial fission and fusion in response to cytokine treatment. *A*: extracts from 3T3-L1 adipocytes treated for 24 h with 1 nM cytokine in complete medium were immunoblotted for optic atrophy 1 (OPA1) or β-actin. *B*: densitometric analysis of OPA1 expression from 3 independent experiments. *C* and *D*: protein levels of dymanin-related protein-1 (DRP-1), mitofusin 2 (MFN2), mitofilin, and β-actin in cytosolic and mitochondrial cellular fractions measured by Western blot (*C*) and protein abundance in the mitochondrial fraction normalized to mitofilin (*D*). $^*P < 0.05$.

Numerous studies aim to unravel the disease progression of type 2 diabetes from the lean insulin-sensitive to the obese insulin-resistant state, yet it is unclear whether mitochondrial dysfunction in the adipocyte will lead to obesity and tissue inflammation or whether the local inflammation is causing mitochondrial dysfunction within the adipocyte. Although the initiating event remains unclear, previous studies in our laboratory show that each of the proinflammatory cytokines analyzed here can dramatically reduce the expression of a number of antioxidants in adipocytes (36), and by-products of oxidative stress can activate macrophage to release proinflammatory cytokines (18), perpetuating the oxidative stress and inflam-

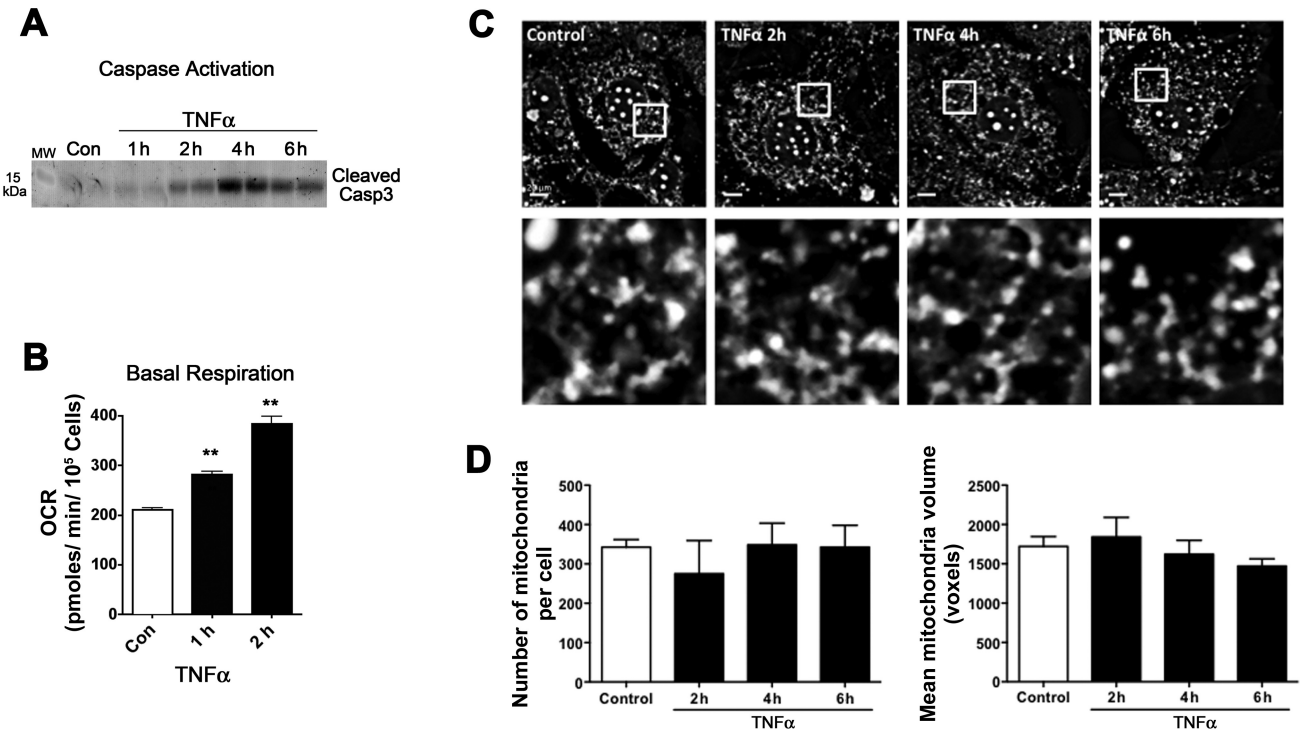

Fig. 8. Acute effects of TNFα on mitochondrial fragmentation. *A*: Western blot of whole cell extract detecting cleaved caspase-3 after no treatment control or 1 nM TNFα for 1, 2, 4, and 6 h. *B*: basal respiration measured by XF24 analyzer in adipocytes (Con) and after 1 nM TNFα for 1–2 h; $n = 3$–5. $^{**}P < 0.001$. *C*: fluorescent microscopy and morphometric analysis of MitoTracker green-stained adipocytes treated or not (Con) for 2, 4, and 6 h with 1 nM TNFα. *D*: cells were scored for mitochondrial no. and mean mitochondrial volume, as reported in Fig. 6; $n = 3$.

mation axis in adipose. The present study was undertaken to determine the effects of three specific inflammatory cytokines that are found to be chronically elevated in obese adipose tissue on mitochondrial function in the adipocyte. Focusing on the common cytokines implicated in adipose biology, TNFα, IL-1β, and IL-6, we found that each cytokine leads to mitochondrial dysfunction, yet the mode of action and cellular outcome is unique for each.

Mitochondrial respiration and cellular metabolism. In our studies, TNFα treatment of 3T3-L1 adipocytes results in a number of dramatic cellular changes linking oxidative stress to altered mitochondrial metabolism and dynamics. There are two known receptors for TNFα (TNFR1 and TNFR2), and both are expressed in adipose tissue. Although both membrane-bound and soluble forms signal through TNFR1, only the membrane-bound form is able to signal through TNFR2 (10). TNFα treatment of adipocytes led to a significant increase in C16 and C18:1 ceramide synthesis as well as an increase in sphinganine (Fig. 4). Ceramides, along with their derivatives, are known to interact with Bcl family members to induce mitochondrial outer membrane permeability. Increased outer membrane permeability allows the release of Cyt *c* into the cytoplasm, which in turn can initiate the apoptosis pathway through caspase activation (22). This process appears to occur selectively in TNFα treatment of adipocytes, as demonstrated by increased ceramides (Fig. 4), the loss of Cyt *c* (Fig. 5, *B* and *C*), and an increase in activated/cleaved caspase-3 (Fig. 6, *E* and *F*), none of which were observed in interleukin treatments. These data suggest that TNFα exposure would lead to high levels of adipocyte apoptosis. However, there are reports of several control measures in place to limit cell death (26). For example, TNFR2 is highly induced in adipose from genetic obesity models (27, 31), and since this receptor lacks the death domain, it may play a prosurvival role to combat apoptotic signaling that arises with the increased TNFα in obese adipose.

Accompanying the changes in ceramide levels, TNFα treatment leads to a shift in the cellular redox status shown by the decreased NAD^+/NADH ratio (Fig. 2*C*). Cellular respiration was increased at 24 h, followed by a decrease by 96 h (Fig. 1). TNFα increased proton leak and diminished $\Delta\Psi_m$ while causing a significant decrease in ATP-coupled respiration at 48 and 96 h. Although increased proton leak could be sufficient to decrease $\Delta\Psi_m$ (6), we cannot rule out other effects, such as increased permeability to explain $\Delta\Psi_m$ loss. These actions could be mediated by TNFα directly or by other intermediates such as ceramides. Interestingly, the synthetic ceramide analog C2 ceramide was described to have similar effects on cardiomyocytes to that of TNFα in the adipocyte. In the cardiomyocyte study, C2 ceramide stimulated Cyt *c* release from the mitochondria, was accompanied by $\Delta\Psi_m$, and decreased ATP levels prior to cell death (42).

TNFα treatment also increased basal glucose uptake (Fig. 2) and basal ECAR (Fig. 1). All of these data are consistent with TNFα-dependent uncoupling of oxygen consumption and ATP synthesis. This uncoupling leads to a compensatory increase in aerobic glycolysis without complete oxidation, similar to the Warburg effect seen in cancer biology (48, 53). Moreover, Chen et al. (12) reported similar results in 3T3-L1 adipocytes treated with TNFα. They found decreased intracellular ATP levels and decreased $\Delta\Psi_m$, further supporting our mitochondrial dysfunction data. TNFα also resulted in a significant time-dependent loss of perilipin (Fig. 2*B*) that was accompanied by increased fatty acid release, as measured by elevated NEFA efflux at 24 h (Fig. 2*A*). In vivo, constitutive upregulation of lipolysis leads to increased circulating NEFAs in the fed state, perhaps contributing to lipotoxicity in obese subjects (20).

In contrast to the effects mediated by TNFα, IL-1β had less metabolic impact on mitochondrial function. IL-1β signals to activate transcription through c-Jun and NF-κB as well as increase cellular cAMP levels (40). In this study, IL-1β had little impact on basal respiration, ATP-coupled respiration, and proton leak until the latest 96-h time point, where it decreased these parameters (Fig. 1). IL-1β does cause mitochondria dysfunction by reducing the maximum respiratory capacity at all time points measured (Fig. 1*D*). The source of the reduced respiratory capacity remains unknown, but it is not likely a reduction in mitochondrial mass since no differences were detected by microscopy or mitochondrial protein level. The pattern of mitochondrial dysfunction resulting from IL-1β exposure is distinct from that seen with TNFα treatment, highlighting the unique characteristics of each signaling pathway as the primary effectors of these alterations. Similar to TNFα treatment, IL-1β-treated cells did exhibit lower NAD^+/NADH ratios as well as increased glucose uptake, but unlike TNFα, they showed no change in ECAR or $\Delta\Psi_m$ (Figs. 1, *E* and *F*, and 2*D*). After 24-h treatment with IL-1β, 3T3-L1 adipocytes did exhibit diminished levels of perilipin proteins (Fig. 2*B*) and increase basal fatty acid efflux (Fig. 2*A*); however, the decrease in perilipin level was transient and was actually significantly increased by 96 h.

Of the cytokines analyzed in this study, IL-6 is divergent from the others in that it does not directly activate transcription factors NF-κB or c-Jun (12, 33). IL-6 is also controversial in what role it has as an inducer of obesity-linked insulin resistance. Although the expression is highly correlated to adiposity and up to 30% of circulating IL-6 is estimated to be adipose derived in healthy individuals, there are reports of IL-6 having anti-inflammatory roles as well (7, 38). In this study, IL-6 treatment of adipocytes did result in mitochondrial dysfunction at all time points analyzed, as indicated by the reduced mitochondrial respiratory capacity (Fig. 1*D*). However, the cytokine had little effect on other respiratory parameters until the late 96-h time point, when IL-6 treated cells exhibited increased basal, proton leak-induced, and coupled respiration (Fig. 1, *A–C*). The delayed response to IL-6 of basal respiration and proton leak point to a secondary effector, perhaps a target gene of the JAK/STAT pathway. Unlike TNFα or IL-1β, treatment with IL-6 is able to increase ATP turnover (Fig. 1*C*), suggesting an increased energy demand following exposure. IL-6 also reduced the NAD^+/NADH ratio, but again this was observed only after 96 h of treatment, suggesting an indirect effector downstream of the IL-6 signal. IL-6 did not alter adipocyte basal glucose transport, perilipin expression, or lipolysis (Fig. 2). Our results suggest that exposure of adipocytes to 1 nM (20 pg/ml) IL-6 has very little direct effect on adipose metabolism. More focused studies are needed to determine whether IL-6 signaling or a secondary mediator is responsible for changes in mitochondrial function after 96 h. Other studies have demonstrated that infusion with recombinant IL-6 stimulates lipolysis and fat oxidation selectively in the muscle

without metabolic effects in the adipose tissue in humans (55). This work is in agreement with our findings.

Oxidative stress. TNFα treatment led to a biphasic change in the oxidative stress program. At shorter times (24 h), TNFα increased superoxide anion levels and protein carbonylation, whereas at longer time points there was an increase in mitochondrial superoxide, and yet reduced protein carbonylation was observed (Fig. 3). Since elevated $\Delta\Psi_m$ and electron transport are reported to be a major source of superoxide production in the mitochondria (1, 39), it was surprising to detect a sharp rise in mitochondrial superoxide in conjunction with reduced $\Delta\Psi_m$ (Fig. 3, *A* and *F*). However, our data are consistent with the work of Chen et al. (12), who found evidence of decreased $\Delta\Psi_m$ and increased cellular ROS levels using H2-DCFDA staining coupled with flow cytometer or microscopic analyses after chronic TNFα in 3T3-L1 adipocytes. Moreover, one report concluded that dihydrolipoamide dehydrogenase, the E3 shared by α-ketoglutarate dehydrogenase and pyruvate dehydrogenase, is a source of ROS (superoxide and hydrogen peroxide) in the presence of substrate but absence of NAD^+ (47). Since TNFα leads to a reduction in NAD^+ levels (Fig. 2*C*), dihydrolipoamide dehydrogenase offers one possible source for the observed increase in mitochondrial superoxide (Fig. 3*A*). NADPH oxidase is also known to be activated by TNFα treatment (57), and although many have reported increased cellular ROS after TNFα treatment of adipocytes (12, 29), our work demonstrates that there is also an increase in superoxide production within the mitochondria with this potent ROS inducer.

IL-1β elicited no significant alteration of mitochondrial superoxide production or protein carbonylation (Fig. 3), indicating a state of normal oxidative homeostasis with this cytokine. IL-1β did slightly increase C16 ceramide levels at 96 h, S1P at 24 h, and sphinganine at 48–96 h (Fig. 4). However, these increased sphingolipid species were not accompanied by a loss in Cyt *c* or increase in caspase-3 activation, as was measured with TNFα (Fig. 5*B*). In fact, IL-1β did not alter any of the mitochondrial protein levels measured, but it did significantly reduce the expression of eNOS and PGC-1α mRNA (Fig. 5*A*). Importantly, despite the decrease in eNOS and PGC-1α mRNA levels, we find no significant change in mitochondrial mass or morphology (29, 49). These results caution the exclusive use of mRNA profiling as a means to interpret cellular metabolism.

There was also no change observed in mitochondrial superoxide production or protein carbonylation (Fig. 3) after IL-6 treatment. Analysis of sphingolipids after IL-6 treatment did present a varied pattern depending on the lipid species. Whereas sphinganine, S1P, and C16 all remained constant, C24 ceramide was significantly reduced after 24–96 h, and C18:1 was elevated after 48 h of IL-6 treatment (Fig. 4). With regard to ceramide-mediated decrease in $\Delta\Psi_m$, there was a transient loss of Cyt *c* seen at 48 h (Fig. 5*C*) but no change mitochondrial morphology or in caspase-3 activation (Fig. 6).

Mitochondrial dynamics. Inflammatory cytokine treatment had a major effect on both mitochondrial biogenesis and dynamics. Mitochondria are very dynamic and through fusion and fission form vast networks and fragment or divide respectively. In our studies, mRNA expression of mitochondrial biogenesis factors such as PGC-1α and NRF-1 were decreased with TNFα treatment, as were the protein levels of some components of electron transport, Cyt *c*, and COX IV (Fig. 5*C*). However, mRNA expression of Tfam and the protein levels of mitofilin are stable after TNFα treatment (Fig. 5). Despite relatively little change in mitofilin level, mitochondria were significantly more fragmented after TNFα treatment, which was most likely due to the lower levels of the inner membrane fusion protein OPA1, notably a loss of the short isoform (Fig. 7). Recently, the protein OPA1, usually related to mitochondrial fusion, was described in the adipocyte as a regulator of hormone-stimulated lipolysis by acting as an A-kinase anchoring protein on the surface of the lipid droplets. Interestingly, OPA1 was found to interact with perilipin, promoting its stability, as evidenced by perilipin downregulation upon OPA1 gene silencing (44). The role for OPA1 in basal lipolysis was not evaluated in this study, but it is tempting to speculate that a decrease in OPA1 could downregulate perilipin, thus altering lipid droplet protein coating and disrupting lipolysis regulation. Although this could provide a novel explanation for our basal lipolysis increase with TNFα, it does not explain the increased fatty acid efflux and transient perilipin reduction in IL-β-treated cells.

Since mitochondrial morphology results from the equilibrium of the fusion and fission rates (33), either an increase in the rate of fission or a decrease in the rate of fusion can cause a fragmented mitochondrial appearance. OPA1 is processed in response to a variety of stress conditions, and loss of mtDNA, dissipation of $\Delta\Psi_m$, or a decrease in mitochondrial ATP levels all can initiate OPA1 processing by OMA1 (3), among other proteases. Clearly, treatment of 3T3-L1 adipocytes with TNFα creates conditions that are favorable for OPA1 cleavage, but the cause of the diminished short isoform remains undetermined. OPA1 processing is necessary for its function, but an imbalance in the ratio of long to short isoforms can affect its function as mitochondrial fusion protein (25). Thus, this imbalance in OPA1 isoforms could be sufficient to explain the fragmented mitochondria phenotype observed. Although Chen et al. (12) reported increased levels in the fission protein DRP-1 by TNFα treatment, we did not observe similar results. This discrepancy could be due to differences in the antibodies used for immunodetection of DRP-1 or the dose (17 vs. 4 ng/ml) and duration (24 vs. 96 h) of treatment. Since the distribution of DRP-1 is more important than its level of expression when its function as a fission protein is assessed (29) and we did not observe any signs of translocation of DRP-1 to the mitochondria, we believe that OPA1 decrease is sufficient to explain the mitochondrial fragmentation observed in our conditions.

In contrast to TNFα, but consistent with stable fission and fusion protein levels, we were not able to detect any impact of IL-1β or IL-6 on mitochondrial morphology or dynamics (Fig. 6).

Overall, the results reported herein indicate that inflammatory cytokines have unique and distinct influences on mitochondrial respiration, oxidative stress, and dynamics. TNFα most dramatically alters 3T3-L1 adipocyte functions, whereas IL-1β and IL-6 have more modest effects. These results are consistent with findings using TNFα receptor-null mice that exhibit attenuated obesity-linked metabolic dysfunction (46). Moreover, since IL-6 can induce low levels of TNFα synthesis by 3T3-L1 adipocytes, it is not unreasonable to consider that some of the chronic effects of interleukins are mediated by

TNFα production and signaling. As such, although each of the cytokines is considered proinflammatory, TNFα exhibits the most profound influences on mitochondrial function in the 3T3-L1 adipocyte.

ACKNOWLEDGMENTS

We thank the Minnesota Supercomputing Institute for software support in primer design and Kazutoshi Aoyama for technical assistance in flow cytometry as well as Duncan Clarke for the use of the Olympus Deltavision microscope. We also appreciate X. Mai Persson at the CTSA Metabolomics Core at Mayo Clinic for providing technical expertise in mass spectrometry of sphingolipid analyses. A special thanks is extended to Marissa Lee for expert technical support with cell culture.

GRANTS

This work was supported by National Institutes of Health (NIH) Grants RO1-DK-084669 (to D. A. Bernlohr) and P30-DK-050456 (to the Minnesota Obesity Center). M. D. Jensen was supported by UL1-TR000135 from the National Center for Advancing Translational Sciences. J. Kuzmicic was supported by a doctoral scholarship from CONICYT-CHILE. S. Lavandero was supported by FONDAP 15130011, ACT1111, and FONDECYT 1120212 from CONICYT, Chile. M. A. Donoghue was supported by NIH Training Grants T32-DK-007203 and R01-AG-020866.

DISCLOSURES

No conflicts of interest, financial or otherwise, are declared by the authors.

AUTHOR CONTRIBUTIONS

W.S.H. and D.A.B. conception and design of research; W.S.H., J.K., J.S.B., M.A.D., and R.F. performed experiments; W.S.H., J.K., J.S.B., M.A.D., R.F., M.D.J., S.L., E.A.A., and D.A.B. analyzed data; W.S.H., J.K., J.S.B., R.F., M.D.J., S.L., E.A.A., and D.A.B. interpreted results of experiments; W.S.H., J.K., J.S.B., M.A.D., and R.F. prepared figures; W.S.H. and D.A.B. drafted manuscript; W.S.H., J.K., J.S.B., M.A.D., R.F., M.D.J., S.L., E.A.A., and D.A.B. edited and revised manuscript; W.S.H., J.K., J.S.B., M.A.D., R.F., M.D.J., S.L., E.A.A., and D.A.B. approved final version of manuscript.

REFERENCES

1. **Adam-Vizi V.** Production of reactive oxygen species in brain mitochondria: contribution by electron transport chain and non-electron transport chain sources. *Antioxid Redox Signal* 7: 1140–1149, 2005.
2. **Alkhouri N, Gornicka A, Berk MP, Thapaliya S, Dixon LJ, Kashyap S, Schauer PR, Feldstein AE.** Adipocyte apoptosis, a link between obesity, insulin resistance, and hepatic steatosis. *J Biol Chem* 285: 3428–3438, 2010.
3. **Baricault L, Ségui B, Guégand L, Olichon A, Valette A, Larminat F, Lenaers G.** OPA1 cleavage depends on decreased mitochondrial ATP level and bivalent metals. *Exp Cell Res* 313: 3800–3808, 2007.
4. **Blachnio-Zabielska AU, Koutsari C, Tchkonia T, Jensen MD.** Sphingolipid content of human adipose tissue: relationship to adiponectin and insulin resistance. *Obesity (Silver Spring)* 20: 2341–2347, 2012.
5. **Blachnio-Zabielska AU, Persson XM, Koutsari C, Zabielski P, Jensen MD.** A liquid chromatography/tandem mass spectrometry method for measuring the in vivo incorporation of plasma free fatty acids into intramyocellular ceramides in humans. *Rapid Commun Mass Spectrom* 26: 1134–1140, 2012.
6. **Brand MD, Nicholls DG.** Assessing mitochondrial dysfunction in cells. *Biochem J* 435: 297–312, 2011.
7. **Brandt C, Jakobsen AH, Adser H, Olesen J, Iversen N, Kristensen JM, Hojman P, Wojtaszewski JF, Hidalgo J, Pilegaard H.** IL-6 regulates exercise and training-induced adaptations in subcutaneous adipose tissue in mice. *Acta Physiol (Oxf)* 205: 224–235, 2012.
8. **Bremer AA, Jialal I.** Adipose tissue dysfunction in nascent metabolic syndrome. *J Obes* 2013: 393192, 2013.
9. **Byerly MS, Swanson R, Wei Z, Seldin MM, McCulloh PS, Wong GW.** A central role for C1q/TNF-related protein 13 (CTRP13) in modulating food intake and body weight. *PLoS One* 8: e62862, 2013.
10. **Cabal-Hierro L, Lazo PS.** Signal transduction by tumor necrosis factor receptors. *Cell Signal* 24: 1297–1305, 2012.
11. **Carmean CM, Cohen RN, Brady MJ.** Systemic regulation of adipose metabolism. *Biochim Biophys Acta* 1842: 424–430, 2014.
12. **Chen XH, Zhao YP, Xue M, Ji CB, Gao CL, Zhu JG, Qin DN, Kou CZ, Qin XH, Tong ML, Guo XR.** TNF-alpha induces mitochondrial dysfunction in 3T3-L1 adipocytes. *Mol Cell Endocrinol* 328: 63–69, 2010.
13. **Chi H, Flavell RA.** Cutting edge: regulation of T cell trafficking and primary immune responses by sphingosine 1-phosphate receptor 1. *J Immunol* 174: 2485–2488, 2005.
14. **Cildir G, Akincilar SC, Tergaonkar V.** Chronic adipose tissue inflammation: all immune cells on the stage. *Trends Mol Med* 19: 487–500, 2013.
15. **Curtis JM, Grimsrud PA, Wright WS, Xu X, Foncea RE, Graham DW, Brestoff JR, Wiczer BM, Ilkayeva O, Cianflone K, Muoio DE, Arriaga EA, Bernlohr DA.** Downregulation of adipose glutathione S-transferase A4 leads to increased protein carbonylation, oxidative stress, and mitochondrial dysfunction. *Diabetes* 59: 1132–1142, 2010.
16. **Deng Y, Scherer PE.** Adipokines as novel biomarkers and regulators of the metabolic syndrome. *Ann NY Acad Sci* 1212: E1–E19, 2010.
17. **Fernández-Sánchez A, Madrigal-Santillán E, Bautista M, Esquivel-Soto J, Morales-González A, Esquivel-Chirino C, Durante-Montiel I, Sánchez-Rivera G, Valadez-Vega C, Morales-González JA.** Inflammation, oxidative stress, and obesity. *Int J Mol Sci* 12: 3117–3132, 2011.
18. **Frohnert BI, Long EK, Hahn WS, Bernlohr DA.** Glutathionylated lipid aldehydes are products of adipocyte oxidative stress and activators of macrophage inflammation. *Diabetes* 63: 89–100, 2014.
19. **Frohnert BI, Sinaiko AR, Serrot FJ, Foncea RE, Moran A, Ikramuddin S, Choudry U, Bernlohr DA.** Increased adipose protein carbonylation in human obesity. *Obesity (Silver Spring)* 19: 1735–1741, 2011.
20. **Gaidhu MP, Anthony NM, Patel P, Hawke TJ, Ceddia RB.** Dysregulation of lipolysis and lipid metabolism in visceral and subcutaneous adipocytes by high-fat diet: role of ATGL, HSL, and AMPK. *Am J Physiol Cell Physiol* 298: C961–C971, 2010.
21. **Galic S, Oakhill JS, Steinberg GR.** Adipose tissue as an endocrine organ. *Mol Cell Endocrinol* 316: 129–139, 2010.
22. **Ganesan V, Perera MN, Colombini D, Datskovskiy D, Chadha K, Colombini M.** Ceramide and activated Bax act synergistically to permeabilize the mitochondrial outer membrane. *Apoptosis* 15: 553–562, 2010.
23. **Gregor MF, Hotamisligil GS.** Inflammatory mechanisms in obesity. *Annu Rev Immunol* 29: 415–445, 2011.
24. **Grimsrud PA, Picklo MJ, Griffin TJ, Bernlohr DA.** Carbonylation of adipose proteins in obesity and insulin resistance: identification of adipocyte fatty acid-binding protein as a cellular target of 4-hydroxynonenal. *Mol Cell Proteomics* 6: 624–637, 2007.
25. **Griparic L, Kanazawa T, van der Bliek AM.** Regulation of the mitochondrial dynamin-like protein Opa1 by proteolytic cleavage. *J Cell Biol* 178: 757–764, 2007.
26. **Herold C, Rennekampff HO, Engeli S.** Apoptotic pathways in adipose tissue. *Apoptosis* 18: 911–916, 2013.
27. **Hofmann C, Lorenz K, Braithwaite SS, Colca JR, Palazuk BJ, Hotamisligil GS, Spiegelman BM.** Altered gene expression for tumor necrosis factor-alpha and its receptors during drug and dietary modulation of insulin resistance. *Endocrinology* 134: 264–270, 1994.
28. **Holland WL, Brozinick JT, Wang LP, Hawkins ED, Sargent KM, Liu Y, Narra K, Hoehn KL, Knotts TA, Siesky A.** Inhibition of ceramide synthesis ameliorates glucocorticoid-, saturated-fat-, and obesity-induced insulin resistance. *Cell Metab* 5: 167–179, 2007.
29. **Houstis N, Rosen ED, Lander ES.** Reactive oxygen species have a causal role in multiple forms of insulin resistance. *Nature* 440: 944–948, 2006.
30. **Jo J, Shreif Z, Periwal V.** Quantitative dynamics of adipose cells. *Adipocyte* 1: 80–88, 2012.
31. **Keller MP, Choi Y, Wang P, Davis DB, Rabaglia ME, Oler AT, Stapleton DS, Argmann C, Schueler KL, Edwards S, Steinberg HA, Chaibub Neto E, Kleinhanz R, Turner S, Hellerstein MK, Schadt EE, Yandell BS, Kendziorski C, Attie AD.** A gene expression network model of type 2 diabetes links cell cycle regulation in islets with diabetes susceptibility. *Genome Res* 18: 706–716, 2008.
32. **Kotsias F, Hoffmann E, Amigorena S, Savina A.** Reactive oxygen species production in the phagosome: impact on antigen presentation in dendritic cells. *Antioxid Redox Signal* 18: 714–729, 2013.
33. **Kuzmicic J, Del Campo A, López-Crisosto C, Morales PE, Pennanen C, Bravo-Sagua R, Hechenleitner J, Zepeda R, Castro PF, Verdejo HE, Parra V, Chiong M, Lavandero S.** [Mitochondrial dynamics: a potential new therapeutic target for heart failure]. *Rev Esp Cardiol* 64: 916–923, 2011.

34. **Langin D, Dicker A, Tavernier G, Hoffstedt J, Mairal A, Rydén M, Arner E, Sicard A, Jenkins CM, Viguerie N, van Harmelen V, Gross RW, Holm C, Arner P.** Adipocyte lipases and defect of lipolysis in human obesity. *Diabetes* 54: 3190–3197, 2005.
35. **Lee BC, Lee J.** Cellular and molecular players in adipose tissue inflammation in the development of obesity-induced insulin resistance. *Biochim Biophys Acta* 1842: 446–462, 2014.
36. **Long EK, Olson DM, Bernlohr DA.** High-fat diet induces changes in adipose tissue trans-4-oxo-2-nonenal and trans-4-hydroxy-2-nonenal levels in a depot-specific manner. *Free Radic Biol Med* 63: 390–398, 2013.
37. **Miller AF.** Superoxide dismutases: ancient enzymes and new insights. *FEBS Lett* 586: 585–595, 2012.
38. **Mizuhara H, O'Neill E, Seki N, Ogawa T, Kusunoki C, Otsuka K, Satoh S, Niwa M, Senoh H, Fujiwara H.** T cell activation-associated hepatic injury: mediation by tumor necrosis factors and protection by interleukin 6. *J Exp Med* 179: 1529–1537, 1994.
39. **Murphy MP.** How mitochondria produce reactive oxygen species. *Biochem J* 417: 1–13, 2009.
40. **O'Neill LA.** The interleukin-1 receptor/Toll-like receptor superfamily: 10 years of progress. *Immunol Rev* 226: 10–18, 2008.
41. **Parra V, Eisner V, Chiong M, Criollo A, Moraga F, Garcia A, Hartel S, Jaimovich E, Zorzano A, Hidalgo C, Lavandero S.** Changes in mitochondrial dynamics during ceramide-induced cardiomyocyte early apoptosis. *Cardiovasc Res* 77: 387–397, 2007.
42. **Parra V, Moraga F, Kuzmicic J, López-Crisosto C, Troncoso R, Torrealba N, Criollo A, Díaz-Elizondo J, Rothermel BA, Quest AF, Lavandero S.** Calcium and mitochondrial metabolism in ceramide-induced cardiomyocyte death. *Biochim Biophys Acta* 1832: 1334–1344, 2013.
43. **Parra V, Verdejo H, Campo A, Pennanen C, Kuzmicic J, Iglewski M, Hill JA, Rothermel BA, Lavandero S.** The complex interplay between mitochondrial dynamics and cardiac metabolism. *J Bioenerg Biomembr* 43: 47–51, 2011.
44. **Pidoux G, Witczak O, Jarnæss E, Myrvold L, Urlaub H, Stokka AJ, Küntziger T, Taskén K.** Optic atrophy 1 is an A-kinase anchoring protein on lipid droplets that mediates adrenergic control of lipolysis. *EMBO J* 30: 4371–4386, 2011.
45. **Roth Flach RJ, Matevossian A, Akie TE, Negrin KA, Paul MT, Czech MP.** β3-Adrenergic receptor stimulation induces E-selectin-mediated adipose tissue inflammation. *J Biol Chem* 288: 2882–2892, 2013.
46. **Steinberg GR, Michell BJ, van Denderen BJ, Watt MJ, Carey AL, Fam BC, Andrikopoulos S, Proietto J, Görgün CZ, Carling D, Hotamisligil GS, Febbraio MA, Kay TW, Kemp BE.** Tumor necrosis factor alpha-induced skeletal muscle insulin resistance involves suppression of AMP-kinase signaling. *Cell Metab* 4: 465–474, 2006.
47. **Tretter L, Adam-Vizi V.** Alpha-ketoglutarate dehydrogenase: a target and generator of oxidative stress. *Philos Trans R Soc Lond B Biol Sci* 360: 2335–2345, 2005.
48. **Upadhyay M, Samal J, Kandpal M, Singh OV, Vivekanandan P.** The Warburg effect: insights from the past decade. *Pharmacol Ther* 137: 318–330, 2013.
49. **Valerio A, Cardile A, Cozzi V, Bracale R, Tedesco L, Pisconti A, Palomba L, Cantoni O, Clementi E, Moncada S, Carruba MO, Nisoli E.** TNF-alpha downregulates eNOS expression and mitochondrial biogenesis in fat and muscle of obese rodents. *J Clin Invest* 116: 2791–2798, 2006.
50. **van den Borst B, Schols AM, de Theije C, Boots AW, Köhler SE, Goossens GH, Gosker HR.** Characterization of the inflammatory and metabolic profile of adipose tissue in a mouse model of chronic hypoxia. *J Appl Physiol* 114: 1619–1628, 2013.
51. **van der Bliek AM, Shen Q, Kawajiri S.** Mechanisms of mitochondrial fission and fusion. *Cold Spring Harb Perspect Biol* 5: pii: a011072, 2013.
52. **Varela L, Horvath TL.** Leptin and insulin pathways in POMC and AgRP neurons that modulate energy balance and glucose homeostasis. *EMBO Rep* 13: 1079–1086, 2012.
53. **Warburg O.** On the origin of cancer cells. *Science* 123: 309–314, 1956.
54. **Weisberg SP, McCann D, Desai M, Rosenbaum M, Leibel RL, Ferrante AW.** Obesity is associated with macrophage accumulation in adipose tissue. *J Clin Invest* 112: 1796–1808, 2003.
55. **Wolsk E, Mygind H, Grøndahl TS, Pedersen BK, van Hall G.** IL-6 selectively stimulates fat metabolism in human skeletal muscle. *Am J Physiol Endocrinol Metab* 299: E832–E840, 2010.
56. **Xu X, Arriaga EA.** Chemical cytometry quantitates superoxide levels in the mitochondrial matrix of single myoblasts. *Anal Chem* 82: 6745–6750, 2010.
57. **Yang B, Rizzo V.** TNF-α potentiates protein-tyrosine nitration through activation of NADPH oxidase and eNOS localized in membrane rafts and caveolae of bovine aortic endothelial cells. *Am J Physiol Heart Circ Physiol* 292: H954–H962, 2007.
58. **Yang G, Badeanlou L, Bielawski J, Roberts AJ, Hannun YA, Samad F.** Central role of ceramide biosynthesis in body weight regulation, energy metabolism, and the metabolic syndrome. *Am J Physiol Endocrinol Metab* 297: E211–E224, 2009.
59. **Youle RJ, van der Bliek AM.** Mitochondrial fission, fusion, and stress. *Science* 337: 1062–1065, 2012.